ORIGINAL ARTICLE

Performance evaluation of a double-pipe heat exchanger with uniform and graded metal foams

Xue Chen[1,2] · Xinlin Xia[2] · Chuang Sun[2] · Fuqiang Wang[3] · Rongqiang Liu[1]

Abstract
Metal foam heat exchangers have attracted a great deal of interest in numerous engineering fields due to their superior thermal capabilities. In the present study, the heat transfer characteristics of a double-pipe heat exchanger with metal foam insert are numerically investigated. The Forchheimer-extended Darcy equation and the local thermal non-equilibrium (LTNE) model are used to predict the fluid and energy transports, respectively. Thermal resistance of the interface solid wall is considered, while the porous-solid boundary follows the continuity principles. The commercial software FLUENT with specific user defined functions (UDFs) is adopted to implement the simulation. Configurations with uniform foam structure are firstly used to analyze the effects of flow arrangement, foam structural parameters (porosity and pore density) and thermal conductivity on the heat exchanger effectiveness and total pressure drop. Then, graded foam structure along the radius is proposed to further make use of the heat transfer potential of metal foam. The overall thermal performance with increasing and decreasing arrangements of porosity and pore density is assessed. The results indicate that the counter flow shows good performance, with 37.5% higher than the parallel flow in effectiveness. The effectiveness and total pressure drop present monotonic variation with the foam structural parameters for the uniform designs, while maximum performance factor occurs at 15 PPI. The effectiveness has a reduction after gradual increase to a peak 0.89 with the increasing of thermal conductivity of foam matrix. For the designs of graded foam structure, using lower porosity and small pore density at both side of the inner pipe wall shows better overall performance with the performance factors of 4.41 and 4.54.

Keywords Double-pipe heat exchanger · Metal foam · Uniform and graded designs · Local thermal non-equilibrium

Nomenclature

c_f	Specific heat, J kg^{-1} K^{-1}
C_F	Inertial coefficient
d_p	Pore diameter, m
h_v	Volumetric heat transfer coefficient, W m^{-3} K^{-1}
k	Thermal conductivity, W m^{-1} K^{-1}
K	Permeability, m^2
l	Length of heat exchanger, m
$\dot{m}$	Mass flow rate, kg s^{-1}
p	Pressure, Pa
PP	Pumping power, W
Pr	Prandtl number
q	Heat flux, W m^{-2}
Q	Heat transfer rate, W
Re_d	Reynolds number based on the pore diameter
r_1, r_2, r_3	Radius of heat exchanger, m
R	Dimensionless r coordinate
T	Temperature, K
$\mathbf{U}$	Velocity vector, m s^{-1}
U	Dimensionless velocity
$\forall$	Volumetric flow rate, m^3 s^{-1}
x, r	Coordinates in flow region, m
X	Dimensionless x coordinate

✉ Xue Chen
Hit_chenxue@hit.edu.cn

✉ Chuang Sun
Sunc@hit.edu.cn

1 School of Mechatronics Engineering, Harbin Institute of Technology, 92, West Dazhi Street, Harbin 150001, People's Republic of China

2 School of Energy Science and Engineering, Harbin Institute of Technology, 92, West Dazhi Street, Harbin 150001, People's Republic of China

3 School of Automobile Engineering, Harbin Institute of Technology at Weihai, 2, West Wenhua Road, Weihai 264209, People's Republic of China

Greek symbols

μ_f Dynamic viscosity, kg m^{-1} s^{-1}
ρ Density, kg m^{-3}
ϕ Porosity
ω Pore per inch, PPI
θ Dimensionless temperature
ε Heat exchanger effectiveness

Subscripts

1, 2 Inner and annular pipes
eff Effective
f Fluid
in   Inlet
out Outlet
s Solid
w Wall

1 Introduction

Heat exchangers are very important elements in multitudinous industrial applications. So far, various active and passive methods have been developed to intensify the heat transfer rate in order to control the overall size and total cost. As a passive technique, inserting the high porosity open-cell foams is an effective way and has captured considerable interest [1–3]. The fluid flow and thermal transport within such a fluid-foam system has been extensively investigated, such as foam fully or partially filled tubes, metal foam wrapped pipes, fully or partially filled porous channels, finned metal foam heat sinks, and other configurations [4]. Meanwhile, the promotion in the overall system performance is also demonstrated very well.

In general, for the investigation of forced convection in the foam-fluid thermal systems, most of the researches are conducted with the fundamental geometries (tube, parallel channel and annulus), see Ouyang et al. [5], Dehghan et al. [6], Bağcı et al. [7], Li et al. [8], etc. Only a few studies are performed with the double-pipe heat exchangers, which are the most widely used construction as a foam heat exchanger. With partial filling of the porous media, Alkam and Al-Nimr [9] highlighted that using porous substrates at the inner pipe wall could substantially increase the double-pipe heat exchanger effectiveness, especially at high heat capacity ratios. Allouache and Chikh [10, 11] carried out the thermodynamics analyses to find the optimal operating conditions to minimize the total entropy generation. The individual use and integrated use of porous fins or baffles and pulsating flow in a double-pipe heat exchanger were numerically analyzed by Targui and Kahalerras [12, 13], and they concluded that the technique combining porous baffles and pulsating flow seems to be promising for improving the overall performance. Numerical investigation and sensitivity analysis on the turbulent heat transfer in a

porous double-pipe heat exchanger were presented by Milani Shirvan et al. [14, 15], the effects of Reynolds number, Darcy number and porous substrate thickness were evaluated. The turbulence effects were also reported by Jamarani et al. [16] with partially porous filled heat exchanger. For the situations completely filled with metal foam, Chen et al. [17] characterized and quantified the advantages and drawbacks for this type of device by introducing a performance factor. The above-mentioned studies used the local thermal equilibrium (LTE) model to represent the thermal transport in the foams, neglecting the temperature difference between the fluid and solid phases. However, in most cases, this assumption is not valid and the local thermal non-equilibrium (LTNE) model should be used instead, by separately dealing with the two phases [18–21].

Using the LTNE model, investigations on the thermal performance of double-pipe heat exchanger with foam insert could be rarely found. Zhao et al. [22] derived an analytical solution for the convention inside the metal foam filled heat exchanger with a predefined flux on the interface wall. Du et al. [23] and Xu et al. [24] theoretically analyzed the conjugate heat transfer inside the parallel-flow and contour-flow double-tube heat exchangers fully occupied by metal foam, respectively. Double-pipe alumina foam heat exchanger was designed and tested by Davidson and his co-workers to recover the sensible heat in a high temperature solar thermochemical reactor [25, 26]. The combined utilization of foam guiding vanes and foam substrate was proposed by Alhusseny et al. [27] to augment the overall performance, and the potential of this approach was numerically proved. The previous works all adopt the design of uniform foam structure. And two main structural parameters, porosity and PPI (pore per inch), are usually used to characterize the foam structure features.

Recently, the effect of foam structure arrangement is being noticed and configurations with functionally graded foam structure have been proposed to further improve the system efficiency, which mostly occurs in two forms: multi-layer [28–32] and gradually-varied [33–35] arrangements. Several studies have been done with the graded foam filled tube and parallel channel subjected to constant wall temperature or heat flux. Aluminum foams with uniform and non-uniform (segmented or integrated) pore size were produced using replication technique and tested by Zaragoza and Goodall [28], and higher heat transfer coefficients were achieved by graded pore size. With two horizontal porous layers, Kuznetsov and Nield [29] investigated the effects of LTNE, layered medium, throughflow and internal heating. Meanwhile, the partial filling with double-layer and three-layer gradient metal foams in a tube was numerically investigated by Xu et al. [30, 31]. The arrangements of foam structural parameters were optimized by Zheng et al. [32] and Siavashi et al. [33] for the foam filled conduit under the assumption of local thermal equilibrium,

Fig. 1 Double-pipe heat exchanger filled with metal foam
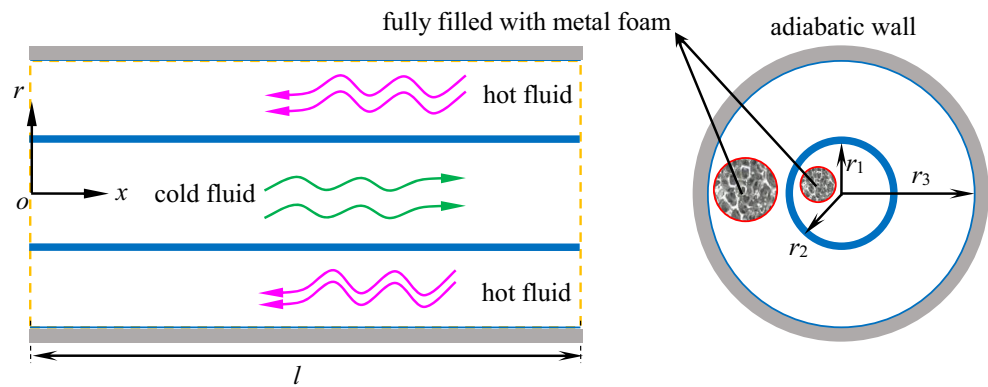
and the stepwise and linear variation profiles of porosity and pore size were both considered by the latter authors. Effects of different porosity gradients and pore-size gradients on the thermal and flow performance were analyzed by Wang et al. [34] for the partially and fully porous filled tubes using the LTE model. Using the LTNE model, Bai et al. [35] addressed that the heat transfer coefficient significantly increases in a channel fully filled with graded foam matrix while the porosity distribution follows a parabolic function. Furthermore, the use of graded foam structure can also be found in the other thermal applications, such as volumetric solar receiver (double-layer [36, 37], three-layer [38, 39], linear distribution [40] and gradually-varied distribution [41]), energy storage with phase changer material (three-layer [42] and linear distribution [43]), and pool boiling (double-layer [44, 45]).

As can be summarized from the literature listed above, various works have be done on the foam filled double-pipe heat exchanger, however, the LTE model is mainly adopted. Besides, few studies can be found using the LTNE model which considers the temperature difference between the foam matrix and fluid, while only uniform design of foam structure is employed. The design of graded foam structure is now receiving a considerable observation, which can be also further used in the double-pipe heat exchanger. Thus, this study focuses on the heat transfer performance of a double-pipe heat exchanger with uniform and graded foam structure. The LTNE model is employed and the coupling effects between the inner and outer pipes are thoroughly considered, as well as the thermal resistance of inner pipe wall. Different graded arrangements of the foam structural properties are discussed.

2 Mathematical model and problem description

The schematic of a double-pipe heat exchanger fully filled with metal foam is shown in Fig. 1. Two streams flow through the inner and annular pipes respectively, and they are separated with a 2.0 mm solid wall. The total length is 400.0 mm and the radii of inner and outer pipes are $r_1 = 20.0$ mm and $r_3 = 42.0$ mm. The flows are steady, incompressible and laminar. The external wall of the outer pipe is thermally insulated and the thickness is excluded in the physical model. The two fluids are assumed to enter the pipes with uniform velocity and temperature, while keeping the same mass flow rate ($\dot{m}_1 = \dot{m}_2$). In the next context, subscripts '1' and '2' are used to represent the inner and annular spaces, respectively. Moreover, a linear distribution of the foam structural parameters (porosity and PPI) from the pipe wall to the freestream is adopted in the research cases of graded foam structure in section 4, and the identical parameter range is considered in both the inner and annular sides.

The fluid flow in the metal foam is described by the Forchheimer-extended Darcy equation. In the two fluid-foam regions, the continuity and momentum equations can be expressed as

$$\nabla \cdot \left(\rho_f \mathbf{U} \right) = 0 \tag{1}$$

$$\frac{1}{\phi^2} \nabla \left(\rho_f \mathbf{U} \cdot \mathbf{U} \right) = -\nabla p$$

$$+ \frac{1}{\phi} \nabla \cdot \left(\mu_f \nabla \mathbf{U} \right) - \frac{\mu_f}{K} \mathbf{U} - \frac{\rho_f C_F}{\sqrt{K}} |\mathbf{U}| \mathbf{U} \tag{2}$$

Table 1 Pertinent parameters for the metal foam filled heat exchanger

Cold fluid	$\rho_{f,1}$ (kg m^{-3})	$c_{f,1}$ (J kg^{-1} K^{-1})	$k_{f,1}$ (W m^{-1} K^{-1})	$\mu_{f,1}$ (kg m^{-1} s^{-1})
	1.205	1005	0.0259	1.81×10^{-5}
Hot fluid	$\rho_{f,2}$ (kg m^{-3})	$c_{f,2}$ (J kg^{-1} K^{-1})	$k_{f,2}$ (W m^{-1} K^{-1})	$\mu_{f,2}$ (kg m^{-1} s^{-1})
	1.0	1009	0.0305	2.11×10^{-5}
Solid	k_w (W m^{-1} K^{-1})	k_s (W m^{-1} K^{-1})	cold inlet (°C)	hot inlet (°C)
	16.3	16.3	20	80

The energy equations of the fluid phase and solid phase within the two pipes are

$$\nabla\cdot\left(\rho_f c_f \mathbf{U} T_f\right) = \nabla\cdot\left[\left(k_{f,eff} + k_d\right)\nabla T_f\right]$$
$$+ h_{sf} a_{sf}\left(T_s - T_f\right) \quad (3)$$

$$\nabla\cdot\left(k_{s,eff}\nabla T_s\right) + h_{sf} a_{sf}\left(T_f - T_s\right) = 0 \quad (4)$$

Besides, the thermal conduction in the interface solid pipe wall can be described as

$$\nabla\cdot(k_w \nabla T_w) = 0 \quad (5)$$

where ρ_f, μ_f and c_f are the fluid density, dynamic viscosity and thermal capacity. ϕ, p, $\mathbf{U}$ and T are the porosity, fluid pressure, superficial velocity and temperature. K and C_F represent the permeability and inertial coefficient. $k_{f, eff}$ and $k_{s, eff}$ are the effective thermal conductivities of the two phases, and k_d is the dispersion conductivity. k_w is the thermal conductivity of the solid pipe wall, and the symbol $h_v = h_{sf} a_{sf}$ denotes the volumetric heat transfer coefficient to couple the two energy equations. For the determination of the above effective transport parameters for metal foams, a detailed review is given by Alhusseny et al. [46]. Here, the effective thermal conductivities are calculated by the following correlations proposed by Boomsma and Poulikakos [47].

$$k_{eff} = \frac{\sqrt{2}}{2(R_A + R_B + R_C + R_D)} \quad (6)$$

where

Fig. 2 Validation of the simulation on the conjugate heat transfer at porous/solid interface when the LTNE model is used

$$R_A = \frac{4\lambda}{[2e^2 + \pi\lambda(1-e)]k_s + [4 - 2e^2 - \pi\lambda(1-e)]k_f},$$

$$R_B = \frac{(e - 2\lambda)^2}{(e - 2\lambda)e^2 k_s + [2e - 4\lambda - (e - 2\lambda)e^2]k_f},$$

$$R_C = \frac{(\sqrt{2} - 2e)^2}{2\pi\lambda^2(1 - 2e\sqrt{2})k_s + 2[\sqrt{2} - 2e - \pi\lambda^2(1 - 2e\sqrt{2})]k_f},$$

$$R_D = \frac{2e}{e^2 k_s + (4 - e^2)k_f}, \text{ and } \lambda = \sqrt{\frac{\sqrt{2}\left(2 - (5/8)e^3\sqrt{2} - 2\phi\right)}{\pi(3 - 4e\sqrt{2} - e)}}, e = 0.339, k_{f,eff} = k_{eff}\big|_{k_f=0}, k_{s,eff} = k_{eff}\big|_{k_s=0}.$$

The heat transfer enhancement due to the fluid mixing in foam structure at the pore scale is considered, and it can be expressed as thermal dispersion. The dispersion conductivity is assumed to be isotropic and computed by the model proposed in Ref. [48] as

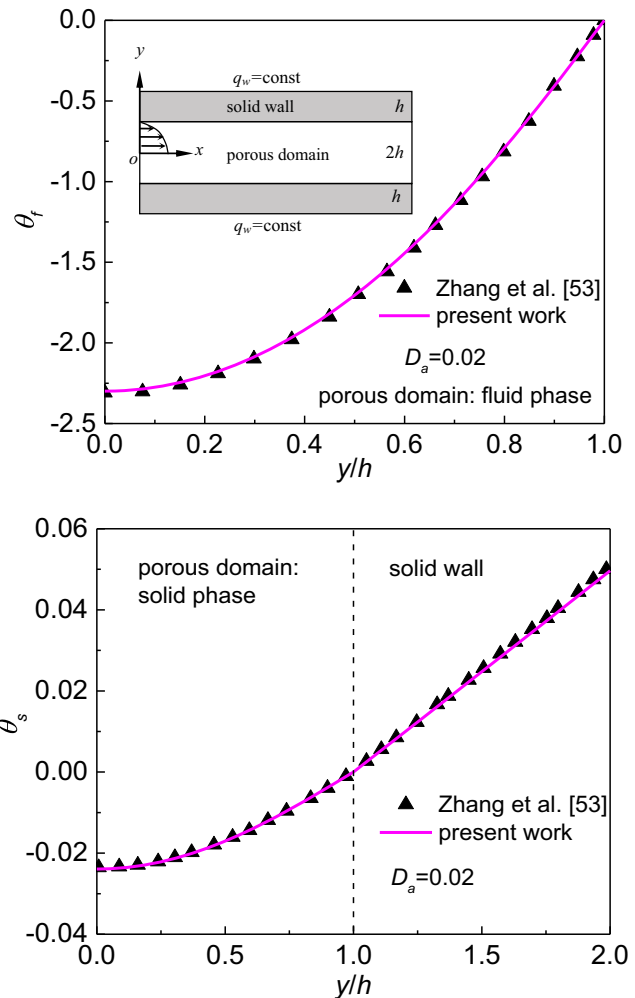$$k_d = C_D \rho_f c_f \sqrt{K} u \quad (7)$$

where $C_D = 0.06$.

Permeability and inertial coefficient are computed according to the model proposed by Calmidi [49] as follows.

$$\frac{K}{d_p^2} = 0.00073(1-\phi)^{-0.224}\left(d_f/d_p\right)^{-1.11} \quad (8)$$

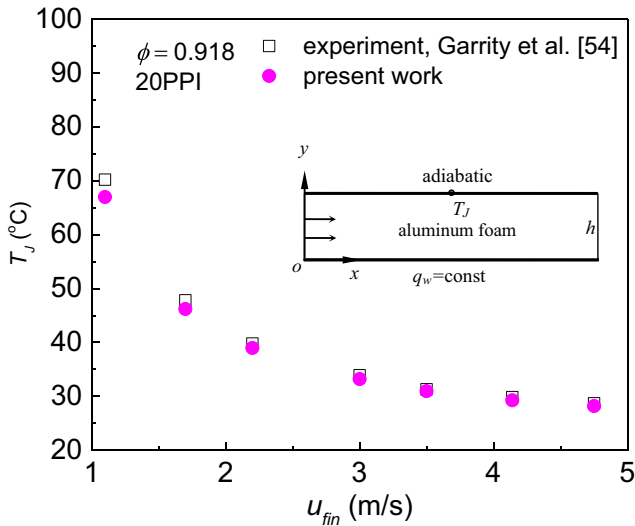$$C_F = 0.00212(1-\phi)^{-0.132}\left(d_f/d_p\right)^{-1.63} \quad (9)$$

Fig. 3 Comparison of the upper surface temperature at $x = 0.5\,l$ with experimental data in Ref. [53]

where $\frac{d_f}{d_p} = 1.18\sqrt{\frac{1-\phi}{3\pi}}\left(\frac{1}{1-e^{-((1-\phi)/0.04)}}\right)$ and $d_p = 0.0254/\omega$.

The empirical model of Zukauskas [50] is employed to compute the interstitial heat transfer coefficient.

$$h_{sf} = \begin{cases} 0.76Re_d^{0.4}Pr^{0.37}k_f/d, & 1 \le Re_d \le 40 \\ 0.52Re_d^{0.5}Pr^{0.37}k_f/d, & 40 \le Re_d \le 10^3 \\ 0.26Re_d^{0.6}Pr^{0.37}k_f/d, & 10^3 \le Re_d \le 2 \times 10^5 \end{cases} \quad (10)$$
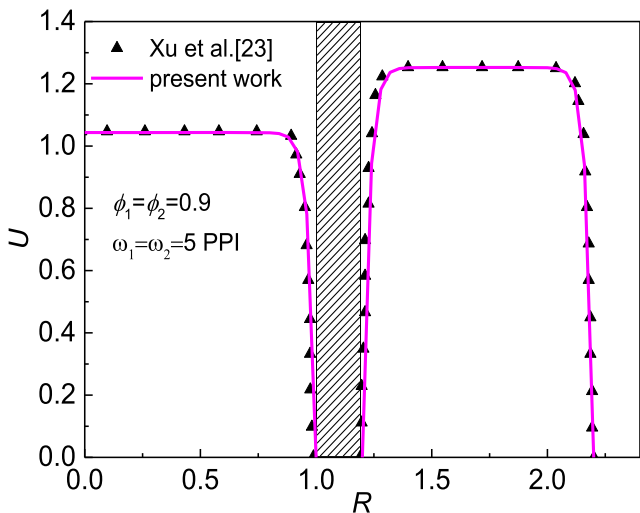

Fig. 4 Comparison of the dimensionless velocity profile with Ref. [23]

where $Re_d = \frac{\rho_f u d}{\mu_f}$, $d = (1 - e^{-((1-\phi)/0.04)})d_f$, and the interfacial surface area is calculated as $a_{sf} = \frac{3\pi d_f\left(1 - e^{-((1-\phi)/0.04)}\right)}{(0.59 d_p)^2}$ [48, 51].

A two-dimensional, axisymmetric model is built. The boundary conditions employed to solve the aforementioned governing equations are given as follows.

$$\text{at } x = 0, \begin{cases} 0 < r < r_1: & u = u_{fin,1}, v = 0, \frac{\partial T_s}{\partial x} = 0, T_f = T_{fin,1} \\ r_1 < r < r_2: & \frac{\partial T_w}{\partial x} = 0 \\ r_2 < r < r_3: & \frac{\partial u}{\partial x} = \frac{\partial v}{\partial x} = \frac{\partial T_f}{\partial x} = \frac{\partial T_s}{\partial x} = 0 \end{cases} \quad (11)$$

$$\text{at } r = 0: \quad \frac{\partial u}{\partial r} = 0, v = 0, \frac{\partial T_s}{\partial r} = \frac{\partial T_f}{\partial r} = 0 \quad (12)$$

$$\text{at } 0 < x < l, \begin{cases} r = r_1, r_2: & u = v = 0, -\left(k_{f,eff} + k_d\right)\frac{\partial T_f}{\partial r} - k_{s,eff}\frac{\partial T_s}{\partial r} = -k_w\frac{\partial T_w}{\partial r}, T_f = T_s = T_w \\ r = r_3: & u = v = 0, -\left(k_{f,eff} + k_d\right)\frac{\partial T_f}{\partial r} - k_{s,eff}\frac{\partial T_s}{\partial r} = 0, T_f = T_s = T_w \end{cases} \quad (13)$$

$$\text{at } x = l, \begin{cases} 0 < r < r_1: & \frac{\partial u}{\partial x} = \frac{\partial v}{\partial x} = \frac{\partial T_f}{\partial x} = \frac{\partial T_s}{\partial x} = 0 \\ r_1 < r < r_2: & \frac{\partial T_w}{\partial x} = 0 \\ r_2 < r < r_3: & u = -u_{fin,2}, v = 0, \frac{\partial T_s}{\partial x} = 0, T_f = T_{fin,2} \end{cases} \quad (14)$$

The inlet temperatures of the two fluids are 20 °C and 80 °C, respectively. The inlet velocity of cold fluid is 0.75 m/s, and that of hot fluid is determined based on the assumption of identical mass flow rate. The pipe wall is made of stainless steel with a conductivity of 16.3 W/(m·K), and the same value is taken for the solid foam matrix as a typical case (such as stainless steel foam and FeCrAlY foam). Additionally, the thermophysical properties in all simulations are regarded to be constant, which are listed in Table 1.

Table 2 Comparison of the two flow arrangements

Arrangement		ε	$\triangle p_t$ (Pa)	pp_t (W)	I
Parallel flow	Without foam	0.13	0.5	4.52e-4	–
	With foam	0.48	194.6	0.19	2.51
Counter flow	Without foam	0.14	0.5	4.52e-4	–
	With foam	0.66	194.6	0.19	3.80

The two main factors concerned in the design process of heat exchanger are the heat exchanger effectiveness (ε) and total pressure drop (Δp_t).

$$\varepsilon = \frac{Q_{ex}}{Q_{\max}} = \frac{\dot{m}_1 c_{f,1}\left(T_{fout,1} - T_{fin,1}\right)}{C\left(T_{fin,2} - T_{fin,1}\right)}$$
$$= \frac{\dot{m}_2 c_{f,2}\left(T_{fout,2} - T_{fin,2}\right)}{C\left(T_{fin,2} - T_{fin,1}\right)} \tag{15}$$

$$\Delta p_t = \Delta p_1 + \Delta p_2 \tag{16}$$

where $C = \min\left(\dot{m}_1 c_{f,1}, \dot{m}_2 c_{f,2}\right)$, Δp_1 and Δp_2 are the pressure drops in the inner and annular sides respectively.

In addition, in order to assess the overall thermal performance, the evaluation criterion introduced by Chen et al. [17] is used here. The performance factor is defined as [17]

$$I = \frac{(Q_{ex}/L - PP_t/L)_{foam} - (Q_{ex}/L - PP_t/L)_{plain}}{(Q_{ex}/L - PP_t/L)_{plain}} \tag{17}$$

where PP_t is the total pumping power, which can be determined using the pressure drop and volumetric flow rate ($\forall$).

$$PP_t = PP_1 + PP_2 = \tilde{V}_1 \Delta p_1 + \tilde{V}_2 \Delta p_2 \tag{18}$$
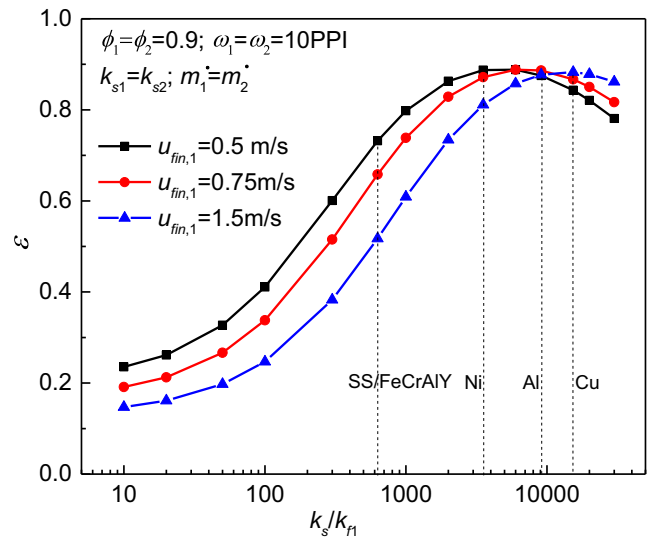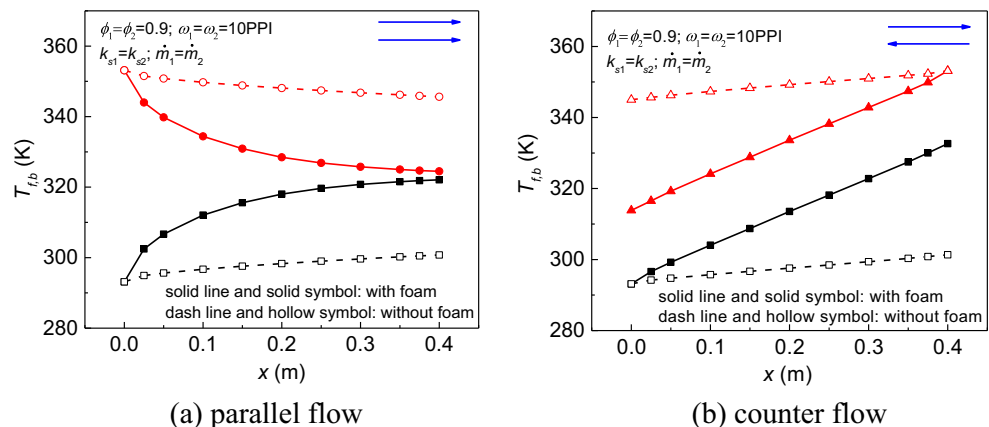

Fig. 6 Effect of foam thermal conductivity on the heat exchanger effectiveness

3 Solution validation

The numerical analysis is performed using the commercial software FLUENT with a two-dimensional axisymmetric model, and the governing equations are solved by the finite-volume method. SIMPLE algorithm is applied to handle the pressure–velocity coupling. Several User Defined Functions (UDFs) are hooked to set the boundary conditions or determine the transport parameters. A non-uniform but structured grid (250 × 65) has been applied after independence check. The convergence criterion of the residual is set to 10^{-10}. During the simulation, the conjugate heat transfer at the interface between porous foam and solid wall should be carefully treated to guarantee the continuity of interfacial temperature and heat flux, while this is automatically satisfied when using the LTE model. When adopting the LTNE model, the boundary condition as Eq. (10) is used, which is presented according to the

Fig. 5 Variation of the bulk fluid temperature along the axial direction for the two flow arrangements

(a) parallel flow

(b) counter flow

Fig. 7 Effect of foam thermal conductivity on the temperature distribution at $u_{fin,\,1} = 0.75$m/s

(a) $x=0.25l$ (b) $x=0.5l$
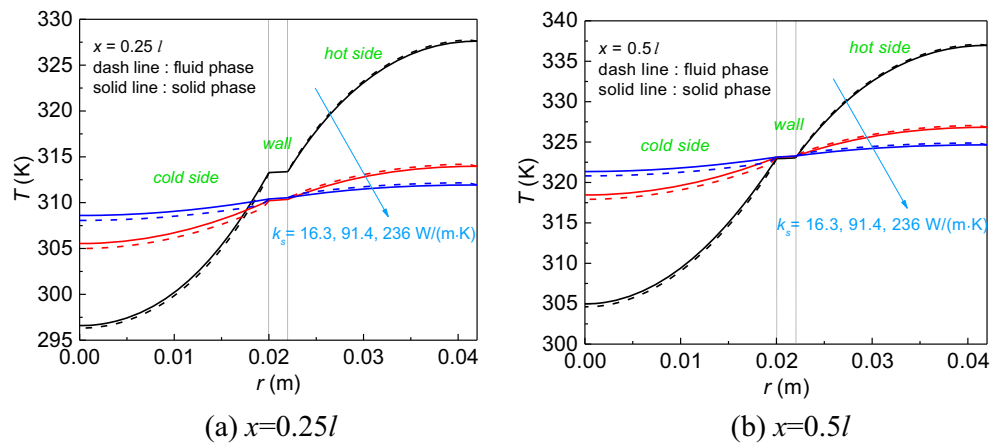
heat flux division between the two constituents [52, 53]. The test case in Ref. [53] is repeated here and compared as shown in Fig. 2. The porosity is 0.95, effective conductivity ratio ($k_{f,\,eff}/k_{s,\,eff}$) is 0.23, Biot number ($Bi = h_v h^2/k_{s,\,eff}$) is 0.025 and Darcy number ($Da = K/h^2$) is 0.02. The dimensionless temperature in Fig. 2 is defined as $\theta = \frac{T - T_{interface}}{q_w h/k_{s,eff}}$.

The modeling of LTNE heat transfer within metal foam is checked against the experiments on forced convection in an aluminum foam filled channel with one side exposed to a constant heat flux [54]. The upper surface temperature is predicted and compared for different inlet velocities at $q_w = 9.77$ kW/m². From Fig. 3, satisfactory agreement between the simulations and experimental data is obtained. Furthermore, the flow in a double-pipe foam heat exchanger is simulated by the Forchheimer-extended Darcy model under the same operating conditions in Ref. [24]. The porosity is 0.9 and pore density is 5 PPI. The velocity profile is displayed in Fig. 4 ($R = r/r_1$, $U = u/u_{fin,\,1}$) and it shows good agreement.

4 Results and discussion

4.1 Heat exchanger performance with uniform foam structure

Two flow arrangements, namely parallel flow and counter flow, are firstly compared at the porosity of 0.9 and pore density of 10PPI. Meanwhile, the similar cases of plain heat exchanger (without metal foam) are also simulated. As exhibited in Table 2, compared with the plain heat exchanger, inserting metal foam has remarkably increased the heat exchanger effectiveness, however, at an expense of pressure drop increment. Compared with the plain heat exchangers, the improvements in effectiveness with foam insert are about 3.7 times (0.48/0.13) and 4.7 times (0.66/0.14) for the two flow arrangements, respectively. The results also reveal that a better performance is reached by the counter flow arrangement, and the effectiveness is 0.48 and 0.66 for the two cases with foam. The effectiveness of counter flow presents (0.66–0.48)/0.48 = 37.5% higher than the parallel flow for the cases with foam, and the performance factors are 3.80 and 2.51 as
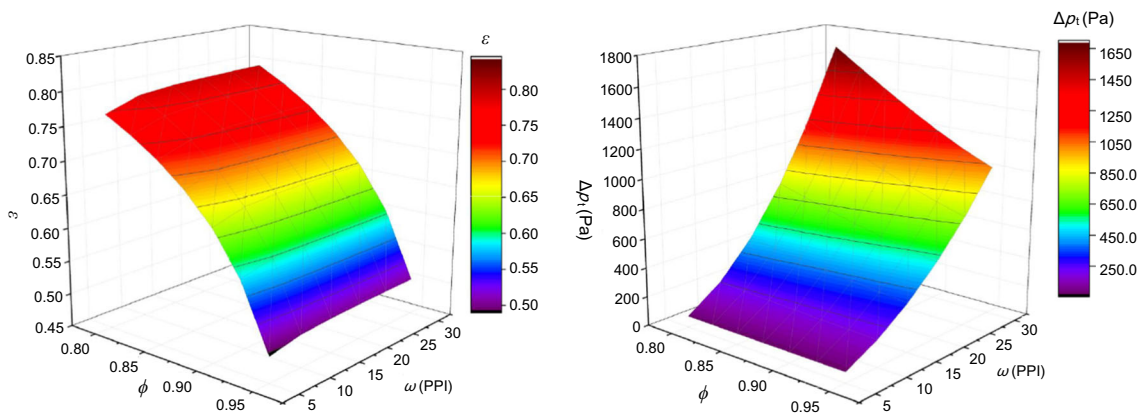

Fig. 8 Effects of the foam structural parameters on the heat exchanger effectiveness and total pressure drop
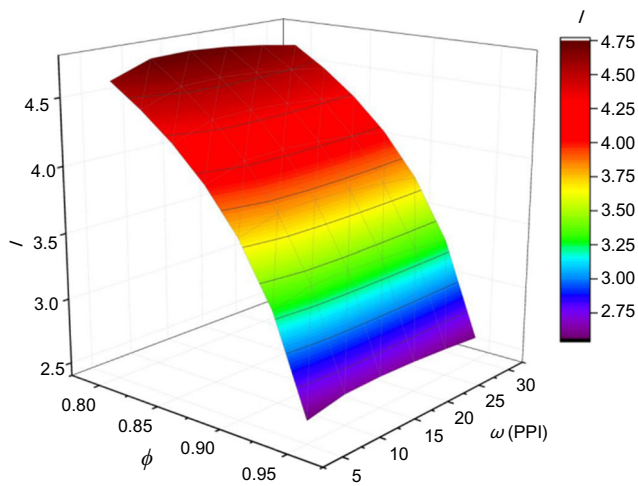
Fig. 9 Performance factor at different combinations of foam structural parameters

Table 3 Some results of configurations with uniform foam structure

Uniform designs	ε	Δp_t (Pa)	pp_t (W)	I
$\phi = 0.8$, $\omega = 10$PPI	0.79	232.5	0.23	4.73
$\phi = 0.95$, $\omega = 10$PPI	0.50	180.9	0.18	2.62
$\phi = 0.9$, $\omega = 5$PPI	0.64	72.1	0.07	3.71
$\phi = 0.9$, $\omega = 30$PPI	0.67	1207.6	1.20	3.75

shown in the table. Besides, the bulk temperature of the fluid phase for different cross sections are plotted in Fig. 5. Nearly linear and asymptotic profiles are respectively obtained by the two flow conditions, and the change trend in the cases with metal foam is more obvious than the cases without metal foam.

Figure 6 demonstrates that the thermal conductivity of foam matrix strongly affects the thermal performance. As the solid phase conductivity of metal foam increases, the heat exchanger effectiveness firstly gradually grows, reaches a peak, and then tends to decrease. The peak values are about 0.89, 0.89 and 0.88 for the three flow rates (represented as inlet velocities of 0.5, 0.75 and 1.5 m/s in the inner pipe).
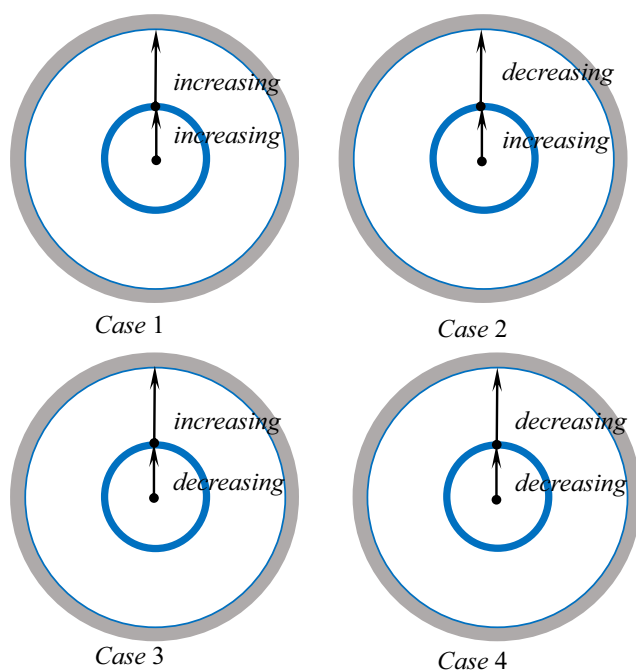

**Fig. 10** Schematic of the four cases with graded foam structure

Besides, the peaks moves towards the larger conductivity as the velocity increases. Before the peak, the thermal resistance along the radial direction is greatly reduced by increasing the conductivity, which promotes the radial heat transfer from hot side to cold side, consequently leading to an increment in effectiveness. However, with further increasing the conductivity, the unexpected decrement trend in effectiveness arises, which is attributed to the enhanced axial thermal conduction. The similar phenomenon here like a 'short-circuiting' is also noticed by Alhusseny et al. [27], namely, more heat is conducted away via annular pipe outlet rather than being transported to the inner pipe across the interface solid wall. This outcome becomes stronger at a lower flow rate (see the curves in Fig. 6). Additionally, the effectiveness is diminished by increasing the flow rate at a fixed low thermal conductivity, whereas the contrary trend occurs when it exceeds a certain high conductivity. Temperature profiles at the cross sections, $x = 0.25 \, l$ and $x = 0.5 \, l$, are displayed in Fig. 7. The temperature gradient along the radius decreases with the increase of thermal conductivity.

Effects of foam structural parameters on the thermal performance are exhibited in Figs. 8 and 9, keeping the other operating conditions unchanged as in Fig. 5a. Generally, monotonic changes in the heat exchanger effectiveness and the total pressure drop are observed with the porosity and pore density, however, the variation in pressure drop is sharper. The maximum effectiveness of 0.79 is achieved by $\phi = 0.8$, $\omega = 30$ PPI with the maximum total pressure drop of 1681.4 Pa. The main reason is that a decrease in porosity can distinctly increase the effective thermal conductivity to augment the heat transfer, simultaneously also increase the fraction of solid phase and flow resistance. Besides, increasing pore density leads to a denser foam matrix, higher flow resistance and also higher volumetric convection heat transfer rate. From Fig. 8, it is clear that the variable amplitude of effectiveness versus porosity is greater than pore density, while contrary tendency occurs in the total pressure drop. According to Fig. 9, a better overall performance (evaluated by performance factor) is obtain by a low porosity, although with a relatively high total pressure drop. The variation of performance factor with pore density is not obvious. Besides, it is found that the peak performance factor occurs at $\omega = 15$PPI at different porosities (0.8~0.95). The maximum performance factor is 4.74 at $\phi =$

Fig. 11 Thermal performance of the configurations with graded porosity design
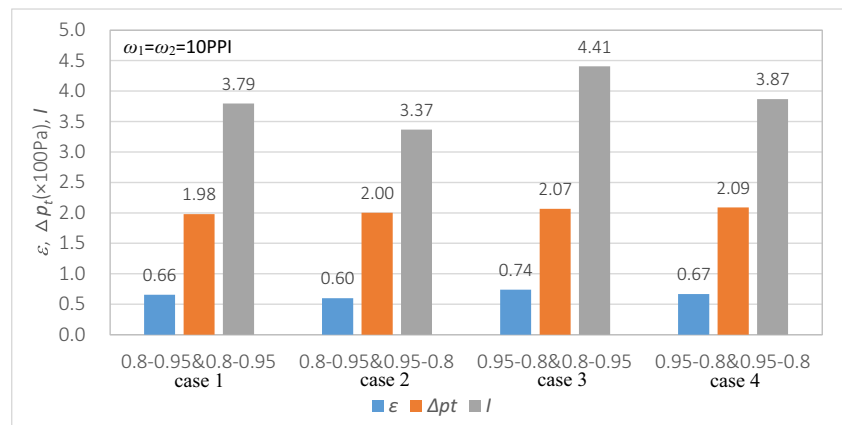
0.8, $\omega = 15$PPI. It can also be seen that the porosity has a stronger influence on the overall performance.

4.2 Heat exchanger performance with graded foam structure

Several studies have outlined that the heat transfer might be improved through proper selection and arrangement of the porosity and pore density, and the graded design of foam structure is proposed as an effective technique. In order to identify the impacts of graded foam structure on the performance of metal foam filled double pipe heat exchanger, here, the linear profiles of porosity or pore density along the radius are analyzed respectively with the ranges of 0.8–0.95 (porosity) and 5–30 PPI (pore density). We use four cases to represent the situations as shown in Fig. 10, namely, case 1: both the inner and annular sides have the increasing arrangement, case 2: increasing in inner pipe while decreasing in annular pipe, case 3: decreasing in inner pipe while increasing in annular pipe, and case 4: both sides have the decreasing arrangement. Two conditions are considered, one is graded porosity at fixed pore density (10 PPI), and the other is graded pore density at fixed porosity (0.9). Besides, some results of uniform foam design are used as a reference (see Table 3).

The graded arrangement of porosity is firstly taken into consideration at a fixed pore density of 10 PPI. Figure 11 illustrates that the maximum effectiveness (0.74) is reached by case 3, nearly the same effectiveness (0.66 and 0.67) is obtained by the cases 1 and 4, and the minimum (0.60) appears in case 2. Besides, the four cases nearly have the same

total pressure drop. By comparison, the variation of performance factor shows the same trend as that of effectiveness, the maximum 4.41 is achieved by cases 3. Combined with the performance factor in Table 3, it can be seen that all the graded designs have better performance than the uniform deign of $\phi = 0.95$, $\omega = 10$ PPI and worse than $\phi = 0.8$, $\omega = 10$ PPI, however holding a lower total pressure drop. It illustrates that the graded design still has a good potential. This figure also indicates that the overall performance mainly depends on the foam layer located at the double sides of the inner pipe wall. Since low porosities (0.8) are attached to the heat transfer surface, the heat transport increases due to the high effective thermal conductivity. For the cases 1 and 4, the porosities nearby the inner pipe are almost the same and the performance factors are close to each other. The permeability is increased by increasing the porosity, and so the maximum velocity magnitude occur near the wall at a high porosity, intensifying the convection heat transfer. However, the thermal conductivity is decreased by increasing the porosity, meaning that a trade off between the convection and conduction exists. Here, the conduction predominates the heat exchange, which overcomes the comparably weaker convective mechanism. Besides, the detailed features are listed in the Table 4.

The temperature distribution along the radial direction is depicted in Fig. 12 for the graded porosity configurations. Similar variation trends are attained by the same graded arrangement used in the inner or annular pipe. Although the temperature gradient is larger with high porosity nearby the inner pipe wall, the effective conductivity is lower, causing a larger gradient in the entire profile and a lower mean temperature in the inner pipe.

Different configurations with graded pore density are simulated at a constant porosity of 0.9, and the results are presented in Fig. 13. The same arrangement in inner pipe has a comparable total pressure drop. Case 3 holds the maximum effectiveness (0.76), and the difference between the cases 1 and 4 is slight, while the minimum 0.57 is obtained by case 2. Combined with the performance factor in Table 3, case 3 also have better performance than the uniform designs with $\phi =$

Table 4 Performance of the different cases with graded porosity design

Graded porosity design	ε	Δp_t (Pa)	pp_t (W)	I
Case 1	0.66	198.1	0.20	3.79
Case 2	0.60	200.2	0.20	3.37
Case 3	0.74	206.8	0.20	4.41
Case 4	0.67	209.0	0.21	3.87

Fig. 12 Temperature profiles at the middle cross section for the different cases with graded porosity design
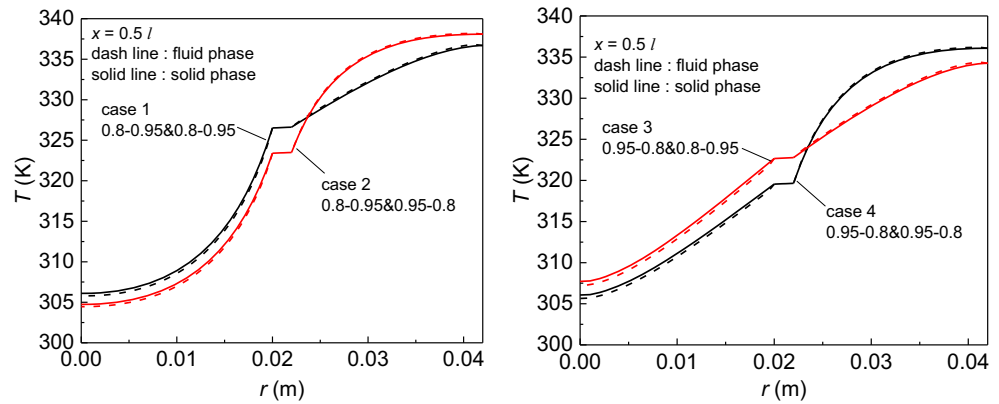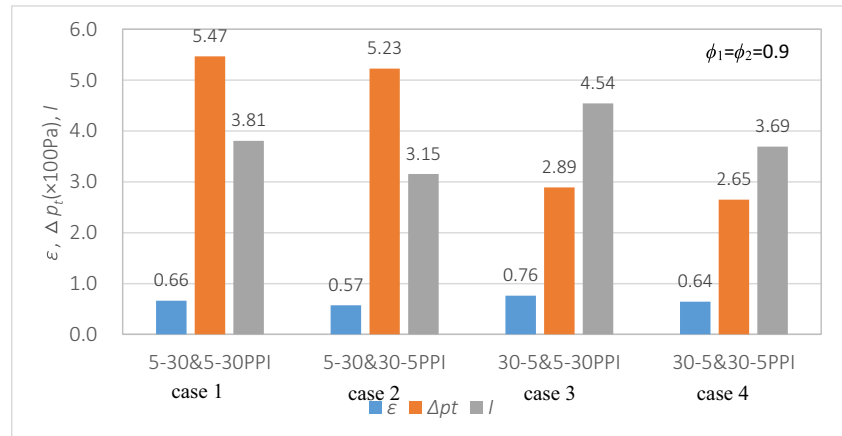

Fig. 13 Thermal performance of the configurations with graded pore density design

0.9, $\omega = 5$ PPI and $\phi = 0.9$, $\omega = 30$ PPI. Here, due to the same porosity is adopted, the thermal resistance of conduction near the interface conducting wall is identical. Therefore, the influence of convection heat transfer plays the predominant role. Since the permeability increases as the pore density decreases, the small pore density increases the velocity magnitude and its gradient near the wall. When more fluid flows near the wall, it transfers more heat from the wall and consequently the heat transfer process improves. Thus, the best performance is achieved by case 3 with a performance factor of 4.54. The detailed parameters are listed in Table 5.

Furthermore, higher pore density has a higher volumetric heat transfer coefficient, yielding a smaller temperature difference between two phases, as illustrated in Fig. 14. On other

Table 5 Performance of the different cases with graded pore density design

Graded pore density design	ε	Δp_t (Pa)	pp_t (W)	I
Case 1	0.66	546.8	0.53	3.81
Case 2	0.57	522.6	0.51	3.15
Case 3	0.76	289.0	0.291	4.54
Case 4	0.64	264.8	0.26	3.69

hand, temperature gradient near the interface conducting wall (inner pipe wall) determines the overall heat transfer, case 3 has a lager gradients at the both sides near the inner pipe wall, due to the high permeability and velocity magnitude nearby the wall.

5 Conclusions

In this study, the thermal performance of metal foam fully filled double-pipe heat exchanger is numerically investigated. The uniform and non-uniform foam structure in the inner and annular pipes are considered and analyzed under the same mass flow rate in both sides. Numerical models of the conjugate heat transfer between two fluids and the LTNE heat transfer between the two phases are fully established. The ranges of the foam structural parameters used here are porosity of 0.8–0.95 and pore density of 5–30 PPI. The main conclusions can be drawn as follows.

(1) The flow arrangement, thermal conductivity and foam structural parameters have significant effect on the thermal performance of heat exchanger. The effectiveness of counter flow with foam insert presents 37.5% higher

Fig. 14 Temperature profiles at the middle cross section for different cases with graded pore density design
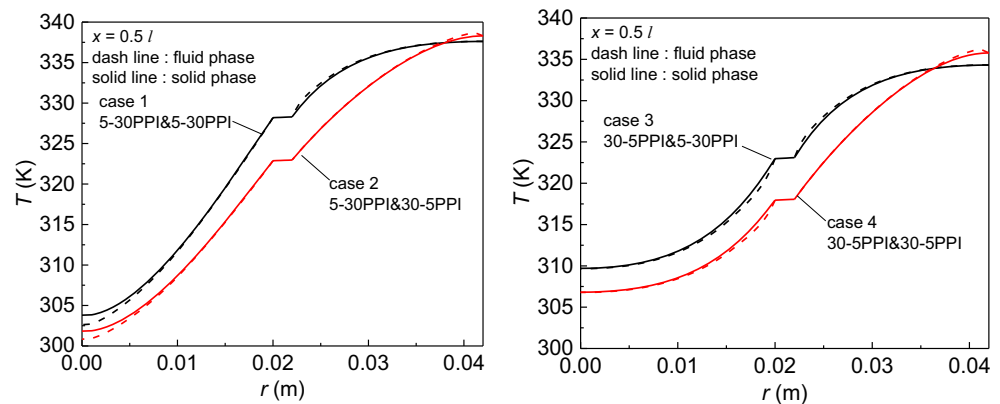
than the parallel flow. The effectiveness firstly increases and then decreases with the increment in solid conductivity rather than steady increasing.

(2) In case of the uniform foam structure, the effectiveness and total pressure drop show monotonic change with the variation in porosity and pore density. Low porosity and large pore density have larger effectiveness and pressure drop, whereas the maximum performance factor occurs at 15 PPI for different porosities.

(3) Configuration with lower porosity attached to the both sides of inner pipe wall holds the best performance in the case of graded porosity design. Besides, for the graded pore density design, a small pore density with high permeability located at the inner pipe wall have improved performance than the other arrangements.

Compliance with ethical standards

Conflict of interest The authors declare that they have no conflict of interest.

References

1. Tan WC, Saw LH, Thiam HS, Xuan J, Cai Z, Yew MC (2018) Overview of porous media/metal foam application in fuel cells and solar power systems. Renew Sust Energ Rev 96:181–197
2. Gong L, Li Y, Bai Z, Xu M (2018) Thermal performance of micro-channel heat sink with metallic porous/solid compound fin design. Appl Therm Eng 137:288–295
3. Buonomo B, di Pasqua A, Ercole D, Manca O, Nardini S (2018) Numerical investigation on aluminum foam application in a tubular heat exchanger. Heat Mass Transf 54:2589–2597
4. Orihuela MP, Shikh Anuar F, Ashtiani Abdi I, Odabaee M, Hooman K (2018) Thermohydraulics of a metal foam-filled annulus. Int J Heat Mass Transf 117:95–106
5. Ouyang XL, Vafai K, Jiang PX (2013) Analysis of thermally developing flow in porous media under local thermal non-equilibrium conditions. Int J Heat Mass Transf 67:768–775
6. Dehghan M, Valipour MS, Saedodin S, Mahmoudi Y (2016) Thermally developing flow inside a porous-filled channel in the presence of internal heat generation under local thermal non-equilibrium condition: a perturbation analysis. Appl Therm Eng 98:827–834
7. Bağcı Ö, Arbak A, De Paepe M, Dukhan N (2018) Investigation of low-frequency-oscillating water flow in metal foam with 10 pores per inch. Heat Mass Transf 54:2343–2349
8. Li PC, Zhong JL, Wang KY, Zhao CY (2018) Analysis of thermally developing forced convection heat transfer in a porous medium under local thermal non-equilibrium condition: a circular tube with asymmetric entrance temperature. Int J Heat Mass Transf 127:880–889
9. Alkam MK, Al-Nimr MA (1999) Improving the performance of double-pipe heat exchangers by using porous substrates. Int J Heat Mass Transf 42:3609–3618
10. Allouache N, Chikh S (2006) Second law analysis in a partly porous double pipe heat exchanger. J Appl Mech 73:60–65
11. Chikh S, Allouache N (2016) Optimal performance of an annular heat exchanger with a porous insert for a turbulent flow. Appl Therm Eng 104:222–230
12. Targui N, Kahalerras H (2008) Analysis of fluid flow and heat transfer in a double pipe heat exchanger with porous structures. Energy Convers Manag 49:3217–3229
13. Targui N, Kahalerras H (2013) Analysis of a double pipe heat exchanger performance by use of porous baffles and pulsating flow. Energy Convers Manag 76:43–54
14. Milani Shirvan K, Ellahi R, Mirzakhanlari S, Mamourian M (2016) Enhancement of heat transfer and heat exchanger effectiveness in a double pipe heat exchanger filled with porous media: numerical simulation and sensitivity analysis of turbulent fluid flow. Appl Therm Eng 109:761–774
15. Milani Shirvan K, Mirzakhanlari S, Kalogirou SA, Öztop HF (2017) Heat transfer and sensitivity analysis in a double pipe heat exchanger filled with porous medium. Int J Therm Sci 121:124–137
16. Jamarani A, Maerefat M, Jouybari NF, Nimvari ME (2017) Thermal performance evaluation of a double-tube heat exchanger partially filled with porous media under turbulent flow regime. Transp Porous Media 120:449–471
17. Chen X, Tavakkoli F, Vafai K (2015) Analysis and characterization of metal foam-filled double-pipe heat exchangers. Numer Heat Transfer A 68:1031–1049
18. Yang K, Vafai K (2011) Transient aspects of heat flux bifurcation in porous media: an exact solution. J Heat Transf 133(5):052602
19. Chen X, Xia XL, Sun C, Yan XW (2017) Transient thermal analysis of the coupled radiative and convective heat transfer in a porous

filled tube exchanger at high temperatures. Int J Heat Mass Transf 108:2472–2480

20. Chen X, Wang FQ, Han YF, Yu RT, Cheng ZM (2018) Thermochemical storage analysis of the dry reforming of methane in foam solar reactor. Energy Convers Manag 158:489–498

21. Gangapatnam P, Kurian R, Venkateshan SP (2018) Numerical simulation of heat transfer in metal foams. Heat Mass Transf 54:553–562

22. Zhao CY, Lu W, Tassou SA (2006) Thermal analysis on metal-foam filled heat exchangers. Part II: tube heat exchangers. Int J Heat Mass Transf 49:2762–2770

23. Du YP, Qu ZG, Zhao CY, Tao WQ (2010) Numerical study of conjugated heat transfer in metal foam filled double-pipe. Int J Heat Mass Transf 53:4899–4907

24. Xu HJ, Qu ZG, Tao WQ (2014) Numerical investigation on self-coupling heat transfer in a counter-flow double-pipe heat exchanger filled with metallic foams. Appl Therm Eng 66:43–54

25. Banerjee A, Bala Chandran R, Davidson JH (2015) Experimental investigation of a reticulated porous alumina heat exchanger for high temperature gas heat recovery. Appl Therm Eng 75:889–895

26. Bala Chandran R, De Smith RM, Davidson JH (2015) Model of an integrated solar thermochemical reactor/reticulated ceramic foam heat exchanger for gas-phase heat recovery. Int J Heat Mass Transf 81:404–414

27. Alhusseny A, Turan A, Nasser A (2017) Rotating metal foam structures for performance enhancement of double-pipe heat exchangers. Int J Heat Mass Transf 105:124–139

28. Zaragoza G, Goodall R (2013) Metal foams with graded pore size for heat transfer applications. Adv Eng Mater 15:123–128

29. Kuznetsov AV, Nield DA (2015) Local thermal non-equilibrium effects on the onset of convection in an internally heated layered porous medium with vertical throughflow. Int J Therm Sci 92:97–105

30. Xu ZG, Qin J, Zhou X, Xu HJ (2018) Forced convective heat transfer of tubes sintered with partially-filled gradient metal foams (GMFs) considering local thermal non-equilibrium effect. Appl Therm Eng 137:101–111

31. Xu ZG, Gong Q (2018) Numerical investigation on forced convection of tubes partially filled with composite metal foams under local thermal non-equilibrium condition. Int J Therm Sci 133:1–12

32. Zheng ZJ, Li MJ, He YL (2015) Optimization of porous insert configurations for heat transfer enhancement in tubes based on genetic algorithm and CFD. Int J Heat Mass Transf 87:376–379

33. Siavashi M, Talesh Bahrami HR, Aminian E (2018) Optimization of heat transfer enhancement and pumping power of a heat exchanger tube using nanofluid with gradient and multi-layered porous foams. Appl Therm Eng 138:465–474

34. Wang B, Hong Y, Hou X, Xu Z, Wang P, Fang X, Ruan X (2015) Numerical configuration design and investigation of heat transfer enhancement in pipes filled with gradient porous materials. Energy Convers Manag 105:206–215

35. Bai X, Kuwahara F, Mobedi M, Nakayama (2018) A forced convective heat transfer in a channel filled with a functionally graded metal foam matrix. J Heat Transf 140:111702

36. Fend T, Pitz-Paal R, Reutter O, Bauer J, Hoffschmidt B (2004) Two novel high-porosity materials as volumetric receivers for concentrated solar radiation. Sol Energy Mater Sol Cells 84:291–304

37. Chen X, Xia X, Meng X, Dong X (2015) Thermal performance analysis on a volumetric solar receiver with double-layer ceramic foam. Energy Convers Manag 97:282–289

38. Roldán MI, Smirnova O, Fend T, Casas JL, Zarza E (2014) Thermal analysis and design of a volumetric solar absorber depending on the porosity. Renew Energy 62:116–128

39. Zhu Q, Xuan Y (2019) Improving the performance of volumetric solar receivers with a spectrally selective gradual structure and swirling characteristics. Energy 172:467–476

40. Wang P, Vafai K (2017) Modeling and analysis of an efficient porous media for a solar porous absorber with a variable pore structure. J Sol Energy Eng 139:051005

41. Du S, Ren QL, He YL (2017) Optical and radiative properties analysis and optimization study of the gradually-varied volumetric solar receiver. Appl Energy 207:27–35

42. Zhu F, Zhang C, Gong XL (2017) Numerical analysis on the energy storage efficiency of phase change material embedded in finned metal foam with graded porosity. Appl Therm Eng 123:256–265

43. Kumar A, Saha SK (2018) Latent heat thermal storage with variable porosity metal matrix: a numerical study. Renew Energy 125:962–973

44. Xu ZG, Zhao CY (2015) Experimental study on pool boiling heat transfer in gradient metal foams. Int J Heat Mass Transf 85:824–829

45. Zhao CY, Xu ZG (2016) Enhanced boiling heat transfer by gradient porous metals in saturated pure water and surfactant solutions. Appl Therm Eng 100:68–77

46. Alhusseny ANM, Nasser AG, Al-zurf NMJ (2018) High porosity metal foams: potentials, applications, and formulations. In: Ghrib T (ed) Porosity: process, technologies and applications. InTechOpen, London

47. Boomsma K, Poulikakos D (2001) On the effective thermal conductivity of a threedimensionally structured fluid-saturated metal foam. Int J Heat Mass Transf 44:827–836

48. Calmidi VV, Mahajan RL (2000) Forced convection in high porosity metal foams. J Heat Transf 122:557–565

49. Calmidi VV (1998) Transport phenomena in high porosity metal foams. University of Colorado: UMI

50. Zukauskas AA (1987) Convective heat transfer in cross-flow. In: Kakac S, Shah RK, Aung W (eds) Handbook of single-phase convective heat transfer. Wiley, New York

51. Lu W, Zhao CY, Tassou SA (2006) Thermal analysis on metal-foam filled heat exchangers. Part I: metal-foam filled pipes. Int J Heat Mass Transf 49:2751–2761

52. Alazmi B, Vafai K (2002) Constant wall heat flux boundary conditions in porous media under local thermal non-equilibrium conditions. Int J Heat Mass Transf 45:3071–3087

53. Zhang HJ, Zou ZP, Li Y, Ye J (2011) Preconditioned density-based algorithm for conjugate porous/fluid/solid domains. Numer Heat Transfer A 60:129–153

54. Garrity PT, Klausner JF, Mei R (2010) Performance of aluminum and carbon foams for air side heat transfer augmentation. J Heat Transf 132:121901